

Supplementary Information (SI)

Electronic Structure Regulation of Carbon Atoms from Wood for Enhancing Zn-Air Batteries Performances

Shengyue Zhang ^a, Zhonghao Chen ^a, Zhong Xiong ^a, Zhicong Wang ^a, Zhihui Zhao ^a, Zhixin Xue

^a, Kang Li ^a, Kai Wang^a, Bin Hui ^{a,*}

^a State Key Laboratory of Bio-Fibers and Eco-Textiles, Shandong Collaborative Innovation Center of Marine Biobased Fiber and Ecological Textile, Institute of Marine Biobased Materials, College of Materials Science and Engineering and College of Chemistry and Chemical Engineering, Qingdao University, Qingdao 266071, P.R. China

** Corresponding author.*

E-mail: huibin@qdu.edu.cn (B. Hui).

Table of Contents

Figure S1. (a and b) SEM images of balsa wood.

Figure S2. (a) Nitrogen adsorption/desorption isotherms and (b) corresponding calculated pore size distribution of CW-900.

Figure S3. XPS mapping of (a) NSCW-800, (b) NSCW-900 and (c) NSCW-1000.

Figure S4. High-resolution C 1s spectrum of (a) NSCW-800, (b) NSCW-900 and (c) NSCW-1000.

Figure S5. High-resolution S 2p spectrum of (a) NSCW-800 and (b) NSCW-1000.

Figure S6. High-resolution N 1s spectrum of (a) NSCW-800 and (b) NSCW-1000.

Figure S7. CV curves of NSCW-900.

Figure S8. Comparison of the activities (E_{onset} and $E_{1/2}$) for NSCW-800, NSCW-900 and NSCW-1000.

Figure S9. OER curves of the catalysts.

Figure S10. Water contact angles of (a) NSCW-800, (b) NSCW-900, (c) NSCW-1000 and (d) CW-900.

Figure S11. LSV curves at different rotating rates for NSCW-900.

Figure S12. K-L plots at different potentials for NSCW-900.

Figure S13. Discharge curves of the Pt/C + RuO₂-based ZAB at various current densities.

Figure S14. Image of the LED powered by two liquid ZABs with NSCW-900.

Table S1. The elemental content of NSCW-800, NSCW-900 and NSCW-1000 from XPS.

Table S2. The ratios of different N species according to XPS results.

Table S3. Summary of the catalytic activities of the reported related electrocatalysts in 0.1 M KOH.

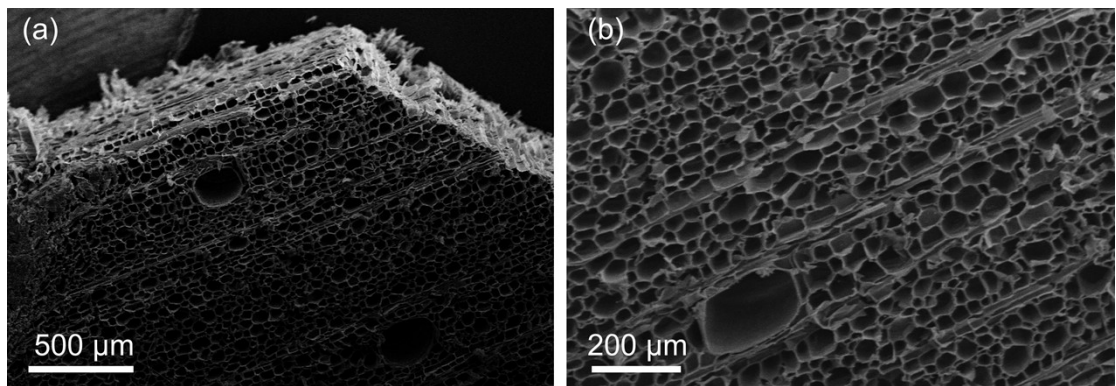


Figure S1. (a and b) SEM images of balsa wood.

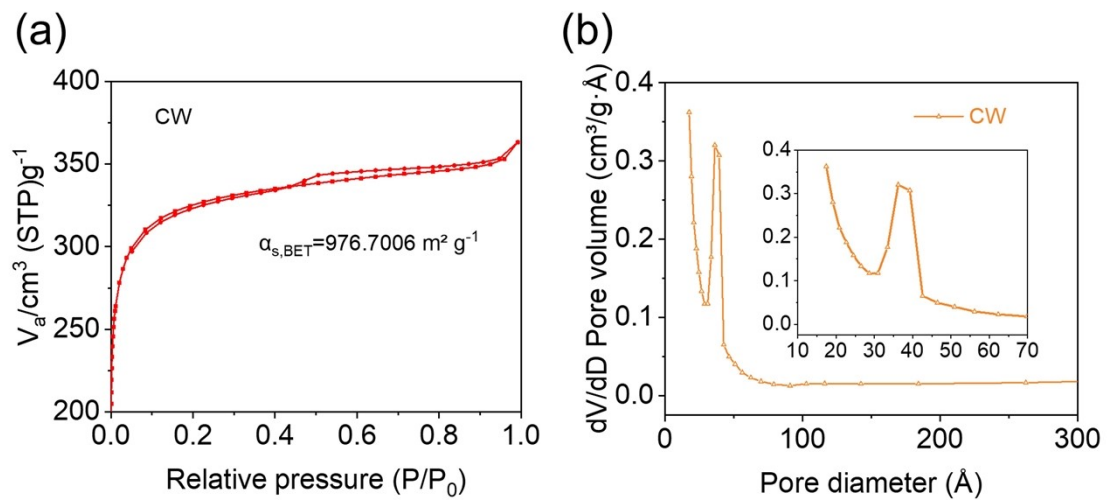


Figure S2. (a) Nitrogen adsorption/desorption isotherms and (b) corresponding calculated pore size distribution of CW-900.

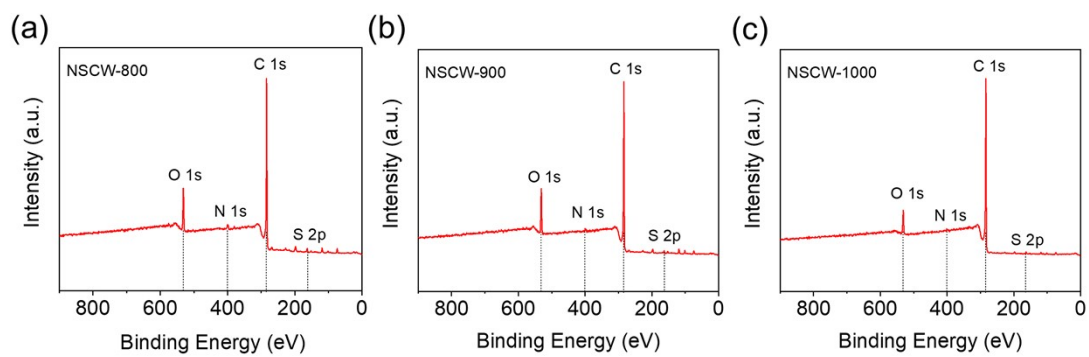


Figure S3. XPS mapping of (a) NSCW-800, (b) NSCW-900 and (c) NSCW-1000.

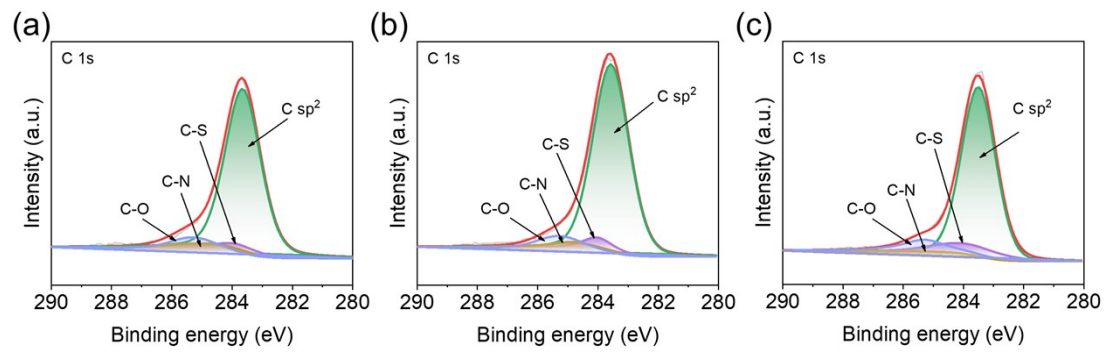


Figure S4. High-resolution C 1s spectrum of (a) NSCW-800, (b) NSCW-900 and (c) NSCW-1000.

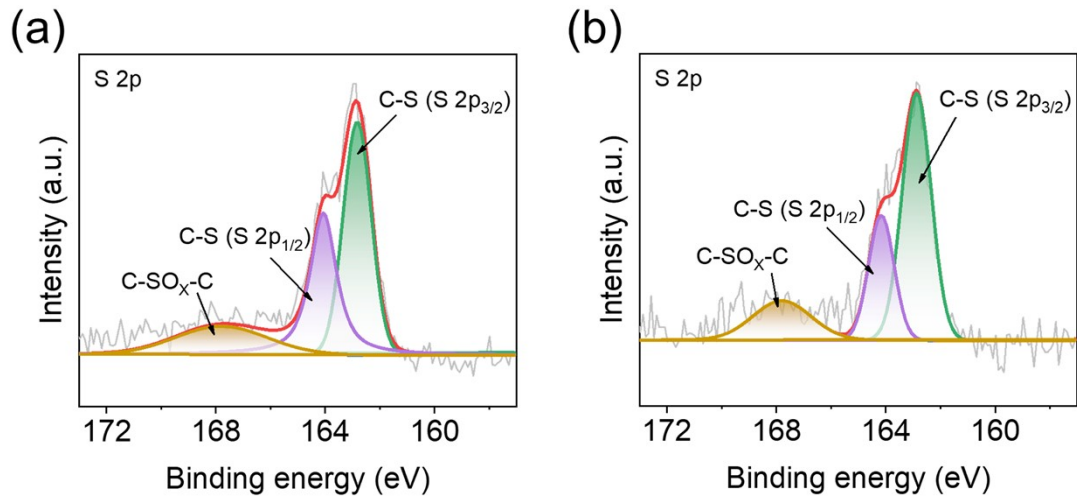


Figure S5. High-resolution S 2p spectrum of (a) NSCW-800 and (b) NSCW-1000.

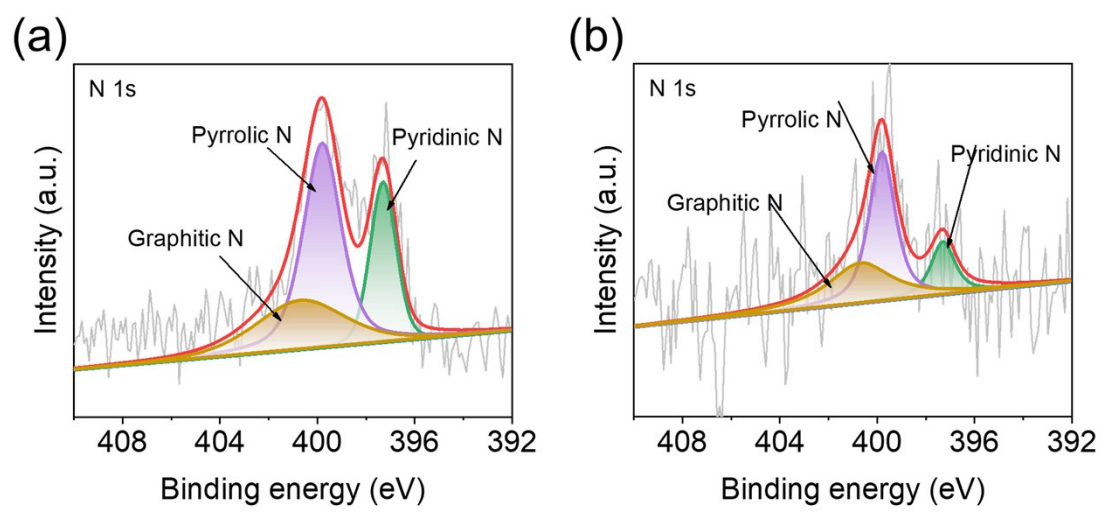


Figure S6. High-resolution N 1s spectrum of (a) NSCW-800 and (b) NSCW-1000.

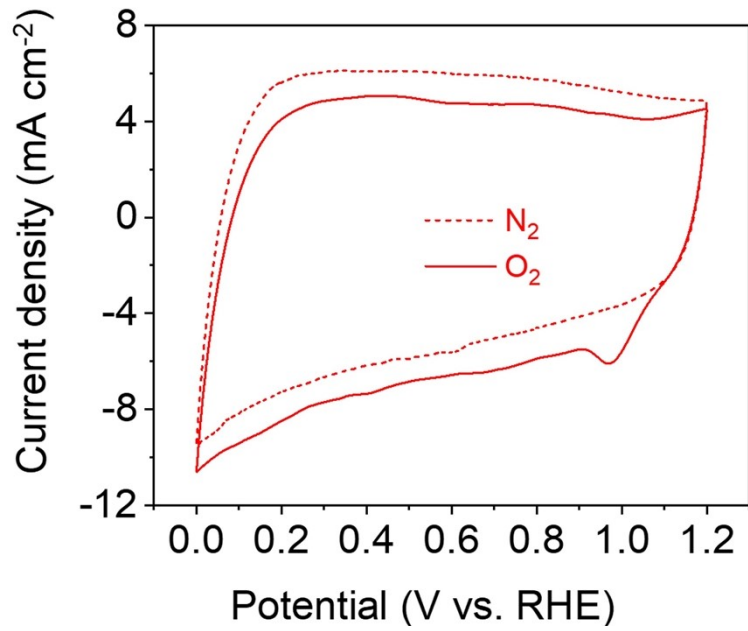


Figure S7. CV curves of NSCW-900.

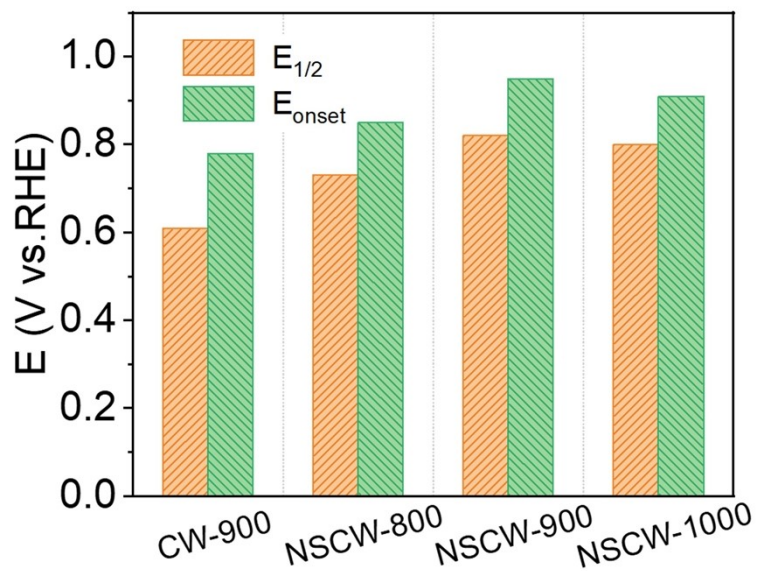


Figure S8. Comparison of the activities (E_{onset} and $E_{1/2}$) for NSCW-800, NSCW-900 and NSCW-1000.

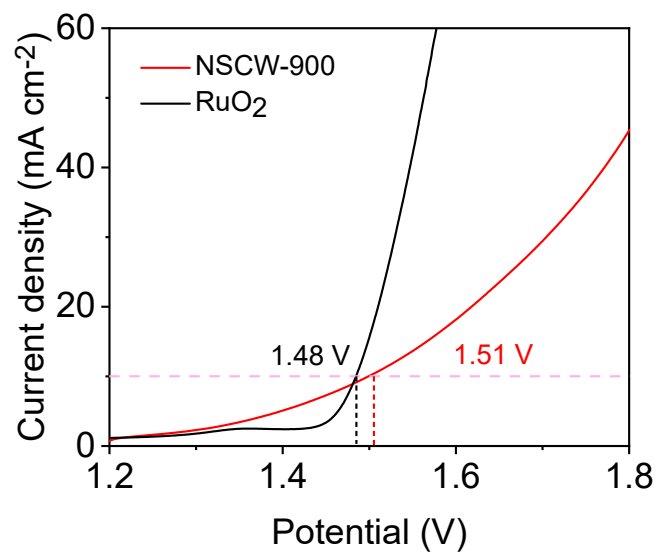


Figure S9. OER curves of the catalysts.

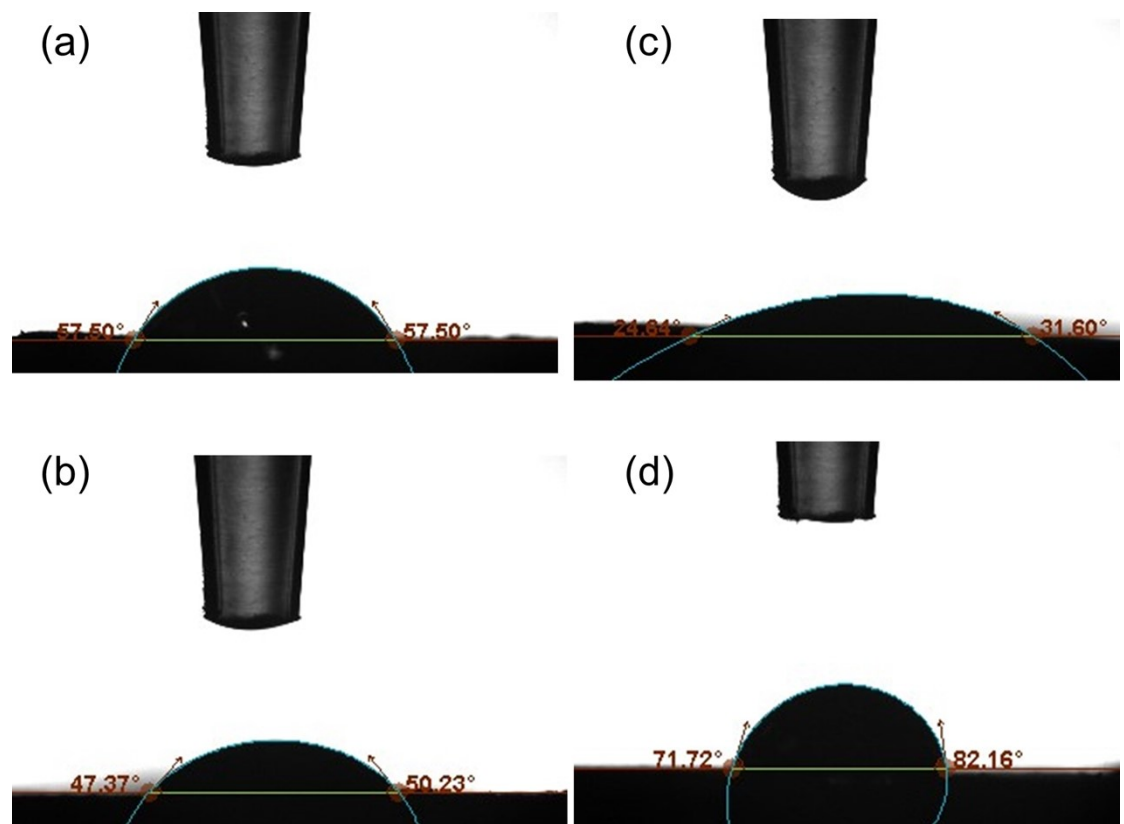


Figure S10. Water contact angles of (a) NSCW-800, (b) NSCW-900, (c) NSCW-1000 and (d) CW-900.

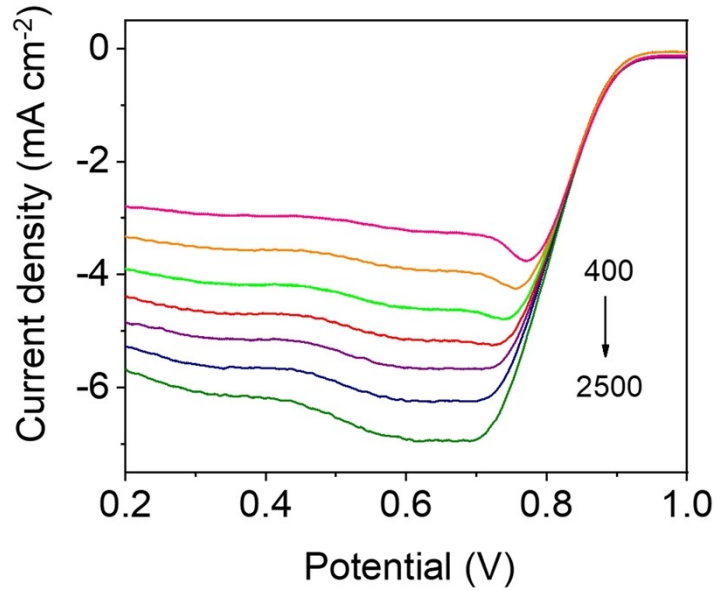


Figure S11. LSV curves at different rotating rates for NSCW-900.

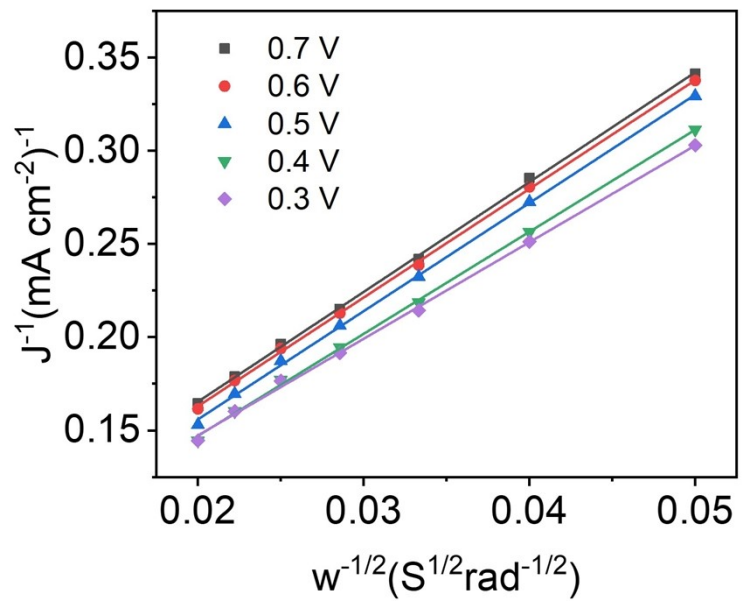


Figure S12. K-L plots at different potentials for NSCW-900.

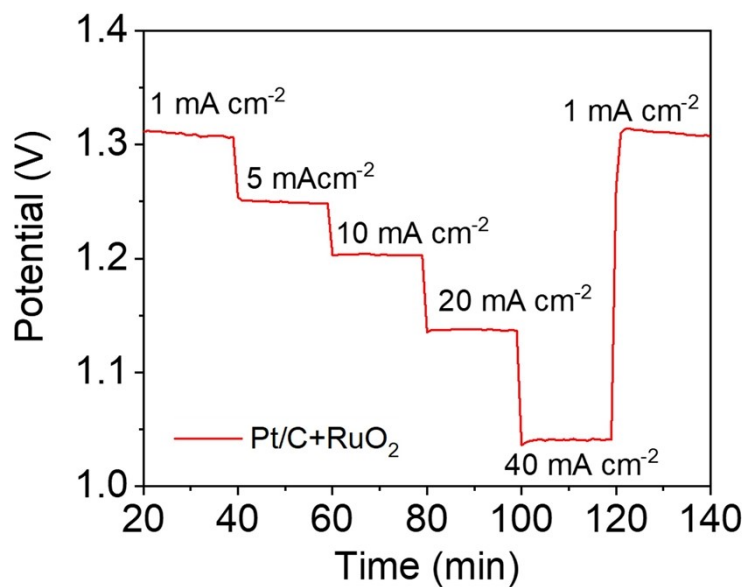


Figure S13. Discharge curves of the Pt/C + RuO₂-based ZAB at various current densities.

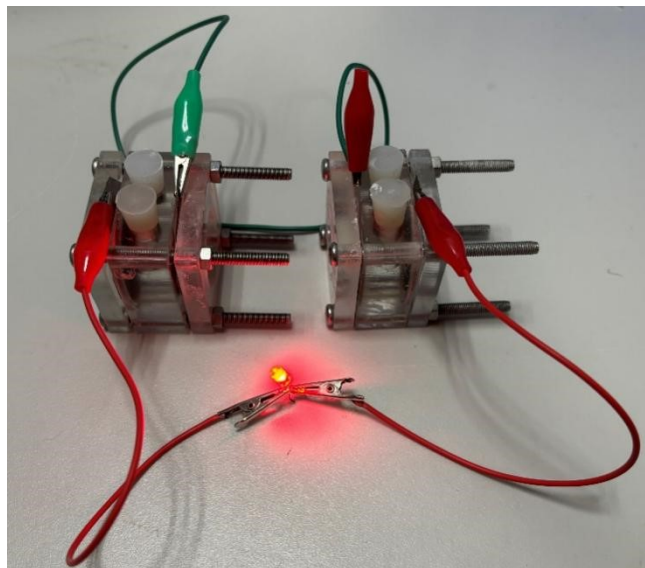


Figure S14. Image of the LED powered by two liquid ZABs with NSCW-900.

Table S1. The elemental content of NSCW-800, NSCW-900 and NSCW-1000 from XPS.

Catalysts	C (At.%)	O (At.%)	N (At.%)	S (At.%)
NSCW-800	82.6	12.72	3.28	1.4
NSCW-900	84.32	12.47	2.33	0.88
NSCW-1000	90.22	6.95	1.96	0.88

Table S2. The ratios of different N species according to XPS results.

Catalysts	Pyridinic N (%)	Graphitic N (%)	Pyrrolic N (%)
NSCW-800	23.7	22.5	53.6
NSCW-900	31.2	25.7	43.1
NSCW-1000	25.8	33.3	42.9

Table S3. Summary of the catalytic activities of the reported related electrocatalysts in 0.1 M KOH.

Catalysts	$E_{1/2}(\text{V})$ (V vs. RHE)	Ref.
NSCW-900	0.832	This work
CN-ZTC	0.81	[1]
NOPHC ₁₀ -900	0.77	[2]
N/S-2DPC-60	0.74	[3]
NBCNT-10	0.82	[4]
RGO	0.79	[5]
N, F-MCFs	0.81	[6]
N-RGO-800	0.72	[7]
BN-CDs	0.77	[8]
BN/C	0.8	[9]
CNT-550-NS	0.81	[10]
NSP-Gra	0.82	[11]

References

- 1 T. Aumont, V. Fogiel, L. L. dos Santos, I. Batonneau-Gener, Y. Pouilloux, C. Comminges, C. Canaff, S. B. C. Pergher, A. Habrioux and A. Sachse, *Mol. Catal.*, 2022, **531**, 8.
- 2 S. C. Huang, Y. Y. Meng, Y. F. Cao, S. M. He, X. H. Li, S. F. Tong and M. M. Wu, *Appl. Catal. B-Environ. Energy*, 2019, **248**, 239-248.
- 3 W. B. Zhang, S. Sun, L. Y. Yang, C. B. Lu, Y. F. He, C. Zhang, M. Cai, Y. F. Yao, F. Zhang and X. D. Zhuang, *J. Colloid Interface Sci.*, 2018, **516**, 9-15.
- 4 P. Wei, X. G. Li, Z. M. He, X. P. Sun, Q. R. Liang, Z. Y. Wang, C. Fang, Q. Li, H. Yang, J. T. Han and Y. H. Huang, *Chem. Eng. J.*, 2021, **422**, 10.
- 5 R. R. Li, F. Liu, Y. H. Zhang, M. M. Guo and D. Liu, *ACS Appl. Mater. Interfaces*, 2020, **12**, 44578-44587.
- 6 T. L. Gong, R. Y. Qi, X. D. Liu, H. Li and Y. M. Zhang, *Nano-Micro Letters*, 2019, **11**, 11.
- 7 H. Miao, S. H. Li, Z. H. Wang, S. S. Sun, M. Kuang, Z. P. Liu and J. L. Yuan, *Int. J. Hydrogen Energy*, 2017, **42**, 28298-28308.
- 8 H. Liu, Z. H. Liu, J. Q. Zhang, L. J. Zhi and M. B. Wu, *New Carbon Mater.*, 2021, **36**, 585-592.
- 9 R. P. Zhao, Q. H. Li, Z. J. Chen, V. Jose, X. Jiang, G. T. Fu, O. M. Lee, S. M. Huang, B, *Carbon*, 2020, **164**, 398-406.
- 10 Y. L. Xu, J. Y. Wang, S. S. Wang, Z. Z. Zhai, B. Ren, Z. Tian, L. H. Zhang, Z. F., Liu, *Int. J. Hydrogen Energy*, 2023, **48**, 34340-34354.

11 Y. X. Wang, N. N. Xu, R. N. He, L. W. Peng, D. Q. Cai, J. L.,Qiao, *Appl. Catal. B-
Environ. Energy*, 2021, **285**, 10.